

UMLE: Unsupervised Multi-discriminator Network for Low Light Enhancement*

Yangyang Qu¹, Kai Chen², Chao Liu³ and Yongsheng Ou³

Abstract—Low-light image enhancement, such as recovering color and texture details from low-light images, is a complex and vital task. For automated driving, low-light scenarios will have serious implications for vision-based applications. To address this problem, we propose a real-time unsupervised generative adversarial network (GAN) containing multiple discriminators, i.e. a multi-scale discriminator, a texture discriminator, and a color discriminator. These distinct discriminators allow the evaluation of images from different perspectives. Further, considering that different channel features contain different information and the illumination is uneven in the image, we propose a feature fusion attention module. This module combines channel attention with pixel attention mechanisms to extract image features. Additionally, to reduce training time, we adopt a shared encoder for the generator and the discriminator. This makes the structure of the model more compact and the training more stable. Experiments indicate that our method is superior to the state-of-the-art methods in qualitative and quantitative evaluations, and significant improvements are achieved for both autopilot positioning and detection results.

I. INTRODUCTION

Enhancing the low-light image is a complex task and has important applications in many fields. For autopilot, taking images in low-light environments severely affects the visual effects and causes a large number of difficulties, such as high noise and loss of image details. For simultaneous localization and mapping (SLAM), low-light images will seriously affect the localization and mapping process. In addition, many advanced tasks such as image instance segmentation and depth estimation will be severely affected. These problems will seriously affect the driving safety of automated vehicles.

Over the last few decades, researchers have developed various theories to achieve the low-light enhancement, and they are categorized into three groups. The first group is based on image histogram equalization [1] and correlation algorithms [2], [3]. This method is useful when both the background and foreground are both too bright or too dark. However, its disadvantage is that it may increase the contrast of background noise and reduce the contrast of useful areas. The second group is based on the retinex theory [4] and its variants [5]–[8]. It adaptively enhances various types of images. However, the processing results are greatly affected by the chromatic aberration variation and noise. The third group

*This work was jointly supported by National Key Research and Development Program of China under Grant 2018AAA0103001, National Natural Science Foundation of China (Grants No. U1613210), Guangdong Special Support Program (2017TX04X265) and Shenzhen Fundamental Research Program (JCYJ20170413165528221)

¹Yangyang Qu, ²Kai Chen, ³Chao Liu and ⁴Yongsheng Ou are with the Shenzhen Institutes of Advanced Technology, Chinese Academy of Sciences, Shenzhen 518055, China. Email: y.s.ou@siaat.ac.cn

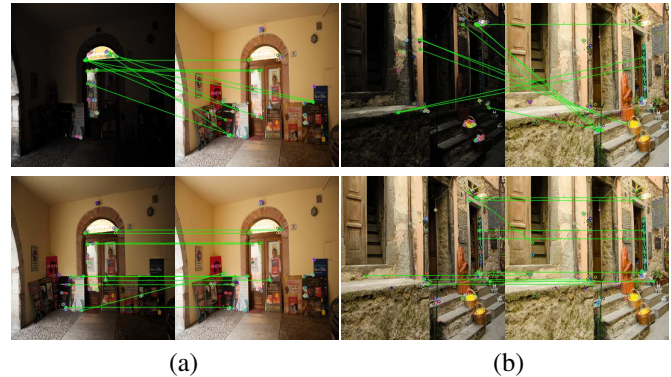


Fig. 1. Results of ORB matching after enhancement of the low-light images by our proposed real-time low-light enhancement method UMLE.

is based on convolutional neural networks and correlation algorithms [9]–[13]. The use of neural network techniques eases image enhancement practice, but the training requires a substantial number of dark-bright-paired images.

This paper proposes a multi-discriminator generative adversarial network (UMLE) to restore the color and texture features of the image. The discriminator consists of three branches. The first branch is a multi-scale discriminator for which image features of different scales can be examined properly. The second branch is a color discriminator that tells whether the color in generated images look real or not. The third branch is a texture discriminator which evaluates the sharpness and clarity of edges in generated images.

We design a network that shares the encoder with the generator and the discriminator. This shared structure reduces the number of model parameters and accelerates the training. Moreover, we design an attention module that puts emphasis on information-rich areas. Via an extensive experimental study, the results indicate our method is qualitatively and quantitatively superior to state-of-the-art methods.

The contributions of this paper are summarized as follows:

- We propose a low-light enhancement GAN. The model's training is independent of paired training data, so it can use images of different scenes and different illuminations. This can effectively improve the generalization and inhibit overfitting.
- We design a multi-branch discriminator which can comprehensively evaluate the image from color, texture, and global information. In addition, we present a novel attention module which combines the channel attention and the pixel attention, and it helps to focus more on the low-light areas.

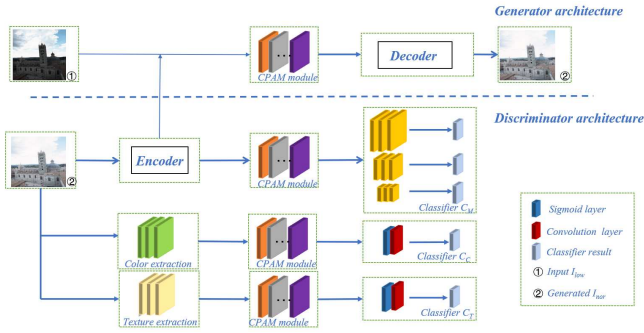


Fig. 2. The architecture of our network. The proposed network consists of two branches. One branch processes the original image, and the second enhances the original image after edge detection. Specific details are described in Sec. Proposed method.

- Our proposed method achieves a significant improvement in automatic driving tasks such as SLAM repositioning and driveable area detection under severe light changes.

II. PROPOSED MODEL

A. Overview

As shown in Fig. 2, we design an unsupervised GAN structure which does not require paired training data to enhance the images. Let L and N be the low-light domain and the normal-light domain. $x \in X_L, X_N$ indicates x from the low-light domain and normal-light domain. Our model studies a transformation from the L domain to the N domain.

Our model contains two generators ($G_{L \rightarrow N}$ transforms low-light image to normal light image, and $G_{N \rightarrow L}$ transforms normal-light image to low-light image) and two discriminators (D_N distinguishes the generated low-light images from the real low-light images, D_L distinguishes the generated normal light images from the real normal light images.) A generator typically includes an encoder and a decoder, whereas a discriminator includes an encoder and a classifier. Different from other related approaches, our generator and discriminator share the same encoder. This approach has been presented in [14]. Due to the shared structure, the training's stability is improved and the model size is reduced.

Because the images' details are largely hidden in the dark, there are color deviations, texture errors, and other problems when generating images. This paper proposes a multi-branch discriminator to solve it, which includes a color discriminator, a texture discriminator, and a multi-scaled discriminator.

B. Channel and Pixel Attention Module (CPA)

A previous study [15] has proved that channel attention can effectively improve the performance of a CNN's performance. Wang et al. [16] demonstrate the avoidance of channel dimensionality can enhance the effect of channel attention. As shown in Fig. 3, we present an attention module which combines the channel attention and the pixel attention.

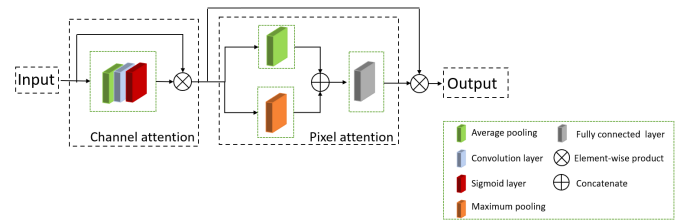


Fig. 3. The architecture of the CPA module. It contains a channel attention module and an attention module. Specific details are described in Sec. Channel and Pixel Attention Module.

The channel attention can achieve channel attention without a dimensionality reduction. First, the module changes the input feature graph from $C \times H \times W$ to $C \times 1 \times 1$ through a channel-wise global average pooling, where C, W, H mean channel dimension, width, and height. Suppose that $\mathcal{X} \in \mathbb{R}^{H \times W \times C}$, the global average pooling can be obtained by:

$$g_c(\mathcal{X}) = \frac{1}{H \times W} \sum_{i=1}^H \sum_{j=1}^W \mathcal{X}_{ij}. \quad (1)$$

Then, the weights of the different channels are obtained by:

$$\omega_c = \sigma(\text{conv}(g_c)), \quad (2)$$

where σ is a sigmoid function, and conv is a convolution function. Finally, the module multiplies the input by the ω_c to obtain the channel attention result:

$$c_r = \omega_c \otimes \mathcal{X}. \quad (3)$$

The pixel attention module can output the pixel attention adaptively. We splice the global average pooling and global max pooling together to obtain the pixel attention feature:

$$p_r = \text{cat}(\sigma(c_r), \gamma(c_r)), \quad (4)$$

where γ is the fully connected function. Then, the pixel attention result is:

$$cp_r = \gamma(p_r) \otimes c_r, \quad (5)$$

and the output is the result of the CPA module.

By adding a residual module in conjunction with CPA, we propose a feature extraction module (CPAM) which can dynamically output the features, and can get better obtain the pixel and channel distribution.

C. Multi-branch Discriminator

The discriminator consists of two parts, encoder E_D and classifier C_D . Through a series of experiments, it can be found that for low-light enhancement, color information and edge information are usually not evident. Using a single discriminator often leads to chromatic aberration, edge blur, and rising overexposure and underexposure problems in local varying illumination. To counter these problems, we put forward a multi-branch discriminator D_M , which consists of three parts.

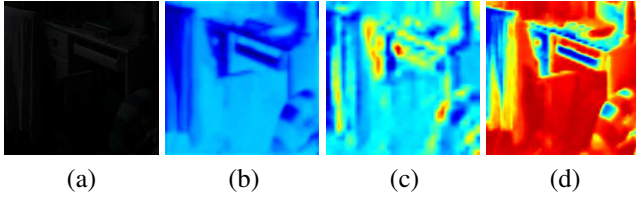


Fig. 4. The feature extraction results of the three discriminators. (a) is the original image, (b) is the visualization of the color discriminator, (c) is the visualization of the texture discriminator, (d) is the visualization of the multi-scale discriminator. It can be found that the results of feature extraction of different discriminators are quite different to combine different discriminators to get better results.

1) *Color discriminator*: The first part is a color discriminator D_c , and its principle design objective is to discriminate the image using the color characteristics. It is supposed to learn the contrast and color differences between the original image I_{ori} and the generated image I_{gen} , while avoiding texture comparisons. Inspired by [6], we adopt the idea of frequency separation. For this part, we apply a Gaussian low-pass filter:

$$G_{x,y} = \lambda \exp\left(-\frac{(x - \mu_x)^2}{2\sigma_x} - \frac{(y - \mu_y)^2}{2\sigma_y}\right), \quad (6)$$

where $\lambda = 0.053$, $\mu_{x,y} = 0$, and $\sigma_{x,y} = 3$. Then features are extracted through the encoder module and the CPAM module to restrain the color distortion, and dynamically output the color features.

2) *Texture discriminator*: The second part is a texture feature discriminator D_T , and its principle design objective is to classify the texture characteristics of the image. Previous attempts have proposed a texture classifier which emulates the process of extracting SIFT descriptors [17]. They convolve it with the two filters to obtain the same x, y gradients for the discriminator in a differentiable manner. In contrast, our method uses a Gaussian high-pass filter. Through this filter, we can extract the image's texture information and avoid the influence of color and other information. Then the feature is extracted through the encode module and the CPAF module, which can make our model better distinguish the image from the perspective of texture.

3) *Multi-scale discriminator*: For the third part, we adopt a multi-scale discriminator D_S . Previous experiments have established that a multi-scale classifier is helpful to improve the effect of discriminators. Different from EnlightenGAN [18] which uses a global-local discriminator, our model trains a three-scale classifier to judge whether the image is real or not. Details in different scales are often need to be enhanced, such as the lightened area. A global classifier cannot pay attention to these regions, for example, to enhance some details present in different scales, such as the lightened area. Providing another two scales in the classifier can focus on different sizes of regions, making the resulting image more realistic. The proposed discriminator contains a local discriminator D_{SL} which is a $10 * 10$ pixel image patch.

In order to intuitively illustrate the function of the three

discriminators, we visualize their results after the CPAM module in Fig. 4. It can be observed that different discriminators pay different attention to the image. The texture discriminator pays more attention to the edge area and texture details of the image, while the color discriminator pays more attention to the whole image. The multi-scale discriminator can extract the color and texture features of the image at the same time.

D. Generator

Because shared structure is adopted, the generator use the same encoder as discriminator. For the decoder, we also adopt the CPAM to extract features. After that, the model can obtain a nice image by up-sampling.

E. Loss function

The following five losses are adopted to train the UMLE model:

1) *Adversarial loss*: We adopt the LSGAN [19] loss as the adversarial loss. This loss matches the distribution of translated images and target images.

$$\mathcal{L}_{adv} = \mathbb{E}_{x \sim \mathcal{X}_N} [\log D_N(x)] + \mathbb{E}_{x \sim \mathcal{X}_L} [\log (1 - D_N(G_{L \rightarrow N}(x)))] \quad (7)$$

2) *Cycle loss*: This loss is adopted to make the image as similar as possible to the original image after two transformations.

$$\mathcal{L}_{cyc} = \mathbb{E}_{x \sim \mathcal{X}_L} [\|x - G_{N \rightarrow L}(G_{L \rightarrow N}(x))\|_1] \quad (8)$$

3) *Color loss*: Color loss forces the enhanced images to have similar color distributions as the target high-quality pictures.

$$\mathcal{L}_{color} = \mathbb{E}_{x \sim \mathcal{X}_L} [\log(D_N(G_{L \rightarrow N}(x)))]. \quad (9)$$

4) *Preserving Loss*: The function of preserving loss is to limit the vgg characteristic distance between the input low light level and its enhanced normal light output.

$$\mathcal{L}_{pre} = \frac{1}{W_i H_i} \sum_{x=1}^{W_i} \sum_{y=1}^{H_i} (\phi_i(x) - \phi_i(G_{L \rightarrow N}(x)))^2, \quad (10)$$

where ϕ_i denotes the i -th feature map extracted from a pre-trained VGG-16 model; and H_i and W_i are the height and width of the feature maps, respectively.

5) *Reconstruction loss*: When the real sample of the source domain is provided as the input of the source domain generator, the transformed image need to be as similar to the real sample.

$$\mathcal{L}_{idt} = \mathbb{E}_{x \sim \mathcal{X}_N} [\|x - G_{L \rightarrow N}(x)\|_1] \quad (11)$$

The whole loss function of our model is as follows:

$$\mathcal{L}_{all} = \omega_1 \mathcal{L}_{adv} + \omega_2 \mathcal{L}_{cyc} + \omega_3 \mathcal{L}_{color} + \omega_4 \mathcal{L}_{pre} + \omega_5 \mathcal{L}_{idt}. \quad (12)$$

In the experiments, we empirically set $\omega_1=1$, $\omega_2=100$, $\omega_3=0.005$, $\omega_4=0.005$, $\omega_5=10$.

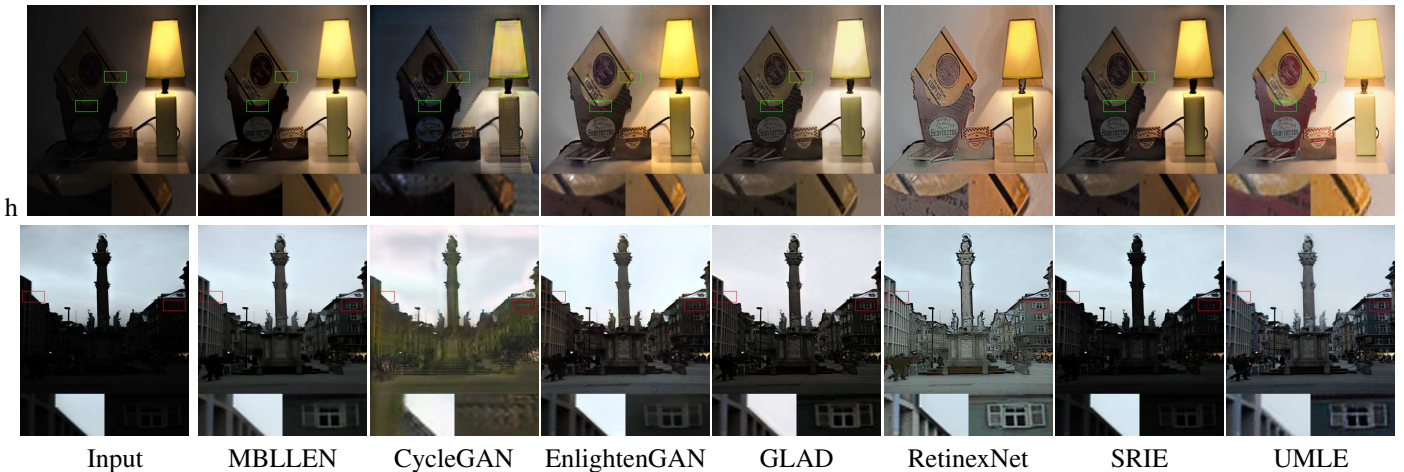


Fig. 5. Visual comparison with state-of-the-art low-light image enhancement methods. Boxes indicate the obvious differences. It can be seen that our results contain little noise and obtain the most natural color of the image.

III. EXPERIMENTS

In this section, we first compare the performance of our method with state-of-the-art image enhancement methods to demonstrate the validity of our proposed method, which consists of experiments (A)–(F). In addition, we demonstrate the utility of our method by applying our method to SLAM relocation and drivable area detection, which are part of the experiments including (G), (H).

A. Dataset

In order to evaluate our method comprehensively, we train it on various scenes including indoor and outdoor scenes. Since our method does not need paired dataset to train, we randomly select images of different scenes and different illuminations from existing datasets which released in [10], [20] and [18]. The dataset includes 923 low light images and 750 normal light images.

For the relocation test, we used the dataset published by ETH [31].

B. Implementation details

We use ReLU [21] as the activation function. The generator and discriminator are trained by AdamGC [22] optimizer, and we use a weight decay at the rate of 0.0001. For the normalization layer, the generator uses Adalin [23] which combines the characteristics of adain [24] and LN [25] which can solve channel unrelated problems. Due to memory constraints, we set the batch size to 1 for our experiments. The training process for our model is carried out on an Nvidia P40. Because our model adopts the method of structure sharing, the training time of our model is greatly reduced. Our models are trained using only 50K iterations.

C. Qualitative Comparison

We conduct extensive qualitative evaluations on typical low-light images with several state-of-art methods. The results are illustrated in Fig. 5. with MBLLEN [26], Cyclegan [27], EnlightenGAN [18], GLAD [28], Retinex-Net [10],

TABLE I
QUANTITATIVE EVALUATION OF LOW-LIGHT IMAGE ENHANCEMENT ALGORITHMS.

Model	NIQE(↓)	ENTROPY(↑)
Retinex-Net	7.539	6.923
MBLLEN	4.481	7.050
GLADNet	3.254	7.340
CycleGAN	4.260	7.092
EnlightenGAN	3.572	7.350
SRIE	4.659	6.874
UMLE	3.485	7.506

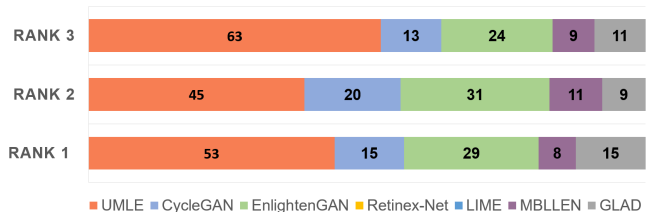


Fig. 6. User study score on the test dataset, the number on the picture means the distribution of the images that the user thinks is the best for each rank.

SRIE [7]. In terms of color and brightness, Enlightengan [18] is prone to color deviation and the result of SRIE [7] is likely to be darker. For texture, LIME [6] generates more noise while enhancing. The results of Cyclegan [27] have the problem of fuzzy details. Retinex-Net [10] produces a kind of effect similar to crayon drawing, which affects the quality of generation. In contrast, our method performs well in terms of texture and color.

D. User study

We adopt a human subjective evaluation [18] which is a human subjective study to compare the performance of our method and other methods. This approach is similar to

TABLE II

THE NUMBER OF PARAMETERS FOR GENERATOR, TRAINING ITERATIONS AND TESTING FPS OF EACH MODEL

Model	Module	Parameters	Training iterations	FPS
EnlightenGAN		22.30M	327k	52
CycleGAN		11.37M	327k	45
ULEN(Our)		16.19M	50k	65

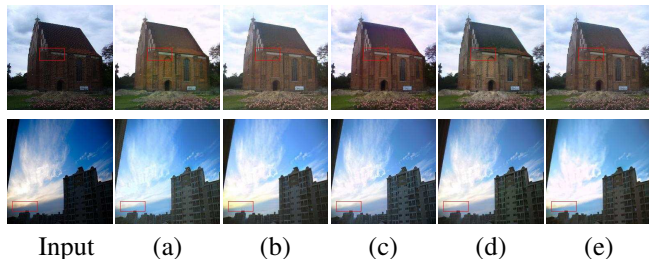


Fig. 7. Visual comparison with ablation results, boxes indicate the obvious differences. (a) is the result without color discriminator, (b) is the result without texture discriminator, (c) is the result without multi-scale discriminator, (d) is the result without CPAF module, (e) is the result of UMLE.

the double stimulus continuous scale. It evaluates the image quality from the following three indicators:

Rank1: How much visible noise the images contain;

Rank2: How much over or under exposure artifacts the images contain;

Rank3: Whether the images show nonrealistic color or texture distortions.

We randomly selected 120 volunteers to evaluate the results. For each indicator, the distributions of the best performing images in all methods are shown in Fig. 6. The number of images that each method performs best in for each category is included in the figure.

By analyzing these results, it can be seen that our method performs best in the three indicators, and our result is natural in color with almost no visible noise.

TABLE III

THE RESULT OF ABLATION STUDY.

Condition	NIQE(↓)	ENTROPY(↑)
with D_C , w/o D_T , w/o D_M	5.416	7.083
with D_T , w/o D_C , w/o D_M	5.656	6.910
with D_M , w/o D_T , w/o D_C	4.840	6.743
with D_T , with D_M , w/o D_C	4.589	7.132
with D_C , with D_M , w/o D_T	3.789	7.291
with D_T , with D_C , w/o D_M	3.929	6.992
with D_M , D_T , D_C , w/o $CPAF$	6.625	7.067
default configuration	3.485	7.506

E. No-reference evaluation

We employ naturalness image quality evaluator (NIQE) [29] and entropy [30] to evaluate the perceptual quality of the

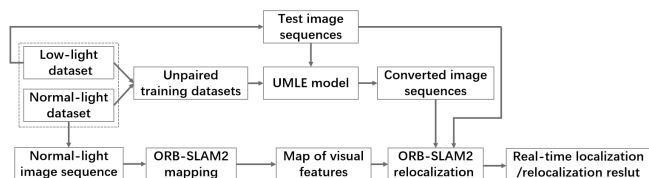


Fig. 8. Flowchart of our experiment. We use the normal illumination image for mapping, while training the UMLE model using the unpaired flashlight illumination image and the normal illumination image. We then test the relocalization on the normal illumination build map using the enhanced image and the original flashlight illumination image, respectively.

state-of-art methods. The NIQE is based on the construction of a series of features used to measure image quality, and lower NIQE [29] values reflect higher quality. The entropy reflects the amount of information carried by the image. The greater the information entropy of the image means the better the quality. Tab. I shows the calculated results of our NIQE [29] and entropy [30] indices. The red result represents the best, blue represents the second best, and bold black represents the third best result. From the table we can see that the proposed UMLE shows well performance in terms of NIQE [29] and entropy [30], and it further demonstrates the advantages of our model in generating normal light images.

In addition, we compare current unsupervised models from the the number of parameters, model training perspective and runtime. Tab. II shows the number of training iterations, generator parameters, and frames per second (FPS) in testing for CylceGAN [27], EnlightenGAN [18], and our method UMLE. All parameters are calculated according to the original article, while we convert the epoch provided to iteration, and parameters means generator parameters, iterations indicates the training iterations and frames per second. Bold black represents the best results. We can see that our method has great advantages in training time, the total number of parameters and testing FPS.

F. Ablation study

To verify the effectiveness of each component proposed in Sec.3, we perform several ablation studies.

We tested the results separately in the absence of each discriminator. In Tab. III we calculate the NIQE [29] value in each case and verify experimentally the importance of each component. The results show that each module contributes substantially to improve the image quality.

In Fig. 7, the results demonstrate the importance of each of component with images, and the data in the table reflect the performance of each condition, where w means without. Through the analysis of the image, we can see that the lack of a color discriminator and a texture discriminator have a great impact on the color and texture. A multi-scale discriminator has a great influence on the whole image generation result. The complete model performs better in visual effect, and the results demonstrate the importance of each component.

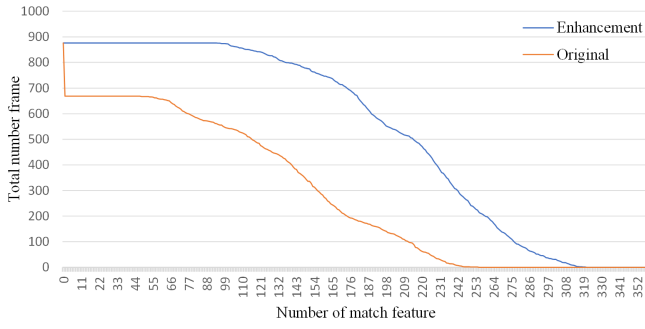


Fig. 9. Comparison of the number of successfully matched feature points before and after image enhancement. The horizontal coordinate represents the number of successful matches, and the vertical coordinate represents the number of images with more features than the corresponding horizontal coordinate. From the image, we can see that the number of features that can be matched in the enhanced image is significantly increased.

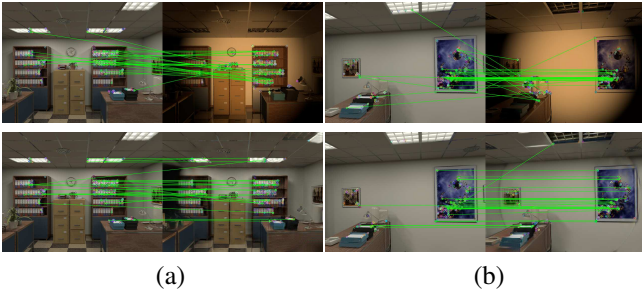


Fig. 10. ORB matching results before and after image enhancement. The first line is the result of matching the flashlight image with the normal light image, and the second line is the result of matching the enhanced image with the normal light image after the UMLE enhancement. We can find that the enhanced image matching results have significant advantages.

G. Localization application

Further, we used the proposed algorithm in a visual map localization application in scenarios with drastic changes in illumination (day→night or light on→off). In the experimental process, we use a publicly available SLAM dataset [31], which is generated by the simulation environment and contains two sets of data for normal and flashlight illumination in the same scene.

The flowchart of our experiment is shown in Fig. 8. First, we randomly extract two types of images of normal light and flashlight from the dataset for training the UMLE network. At the same time, the sequences of continuous images under normal illumination are extracted to construct orb feature maps by using the ORB-SLAM2 [32].

The experiments are mainly to validate our method for the localization problem under drastic light changes. In the localization process, for the pre-built feature map under normal light, we extract five sequence of flashlight images of the same scene at different locations, and try to use them for relocalization. Our localization method is implemented using the relocalization module in ORB-SLAM2 [32]. The results of feature point matching comparison before and after image enhancement can be seen in Fig. 10, and we can see that the enhanced image has a significant improvement on

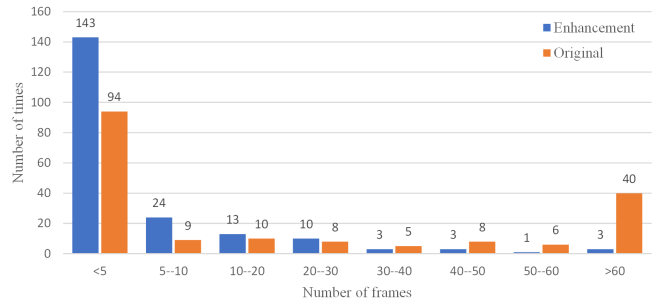


Fig. 11. The number of images required for successful repositioning. The meaning of the horizontal coordinate in the image is the number of images required for successful localization and the meaning of the vertical coordinate is the number of groups of tested sequences in this interval, when the number of images required for successful localization is greater than 60, we consider the localization has failed. From the figure, we can see that the image sequences enhanced by UMLE have a great improvement in both localization success and speed.

the ORB relocation results.

Fig. 9 reflects the number of feature points before and after image enhancement. The number of images is the same, they all start from the same starting point at first. Since the number of successful feature points for many of the original image matches is 0, there is a steep drop at the beginning. We can see from the figure that the number of features matched in the enhanced image is significantly higher than in the original image.

We randomly selected 200 image sequences, each containing 60 images, from the flashlight dataset and the enhancement dataset to test the speed and success of relocalization of these images. The speed of image repositioning is reflected in Fig. 11. We consider a successful match within 5 frames as immediate relocation and a failed relocation above 60 frames.

From Fig. 11, we can see that the success rate of immediate re-localization of the image sequence enhanced with UMLE is 71.5% compared to 47% of the original image, and the success rate of re-localization of the enhanced image is much higher than that of the original image, and the failure rate of relocalization of the enhanced image is 0.15% compared to 20% of the original image, and the failure rate of re-localization of the enhanced image is much lower than that of the original image. This experiment verifies that the speed and success rate of re-localization of the enhanced image are significantly improved under our model.

As can be seen from the experimental results in the images, our proposed method is able to significantly improve the success rate of image matching for the same scene in the case of drastic lighting changes. Our method provides an effective solution to the visual localization problem in scenes with all-weather light changes and is of great practical value.

H. Detection application

Illumination changes have a significant impact on drivable area detection in the autopilot task, so we attempt to apply our model to a night and day conversion task. We test on the Oxford dataset [17]. From the results which are shown in Fig. 12, it can be seen that UMLE can achieve a

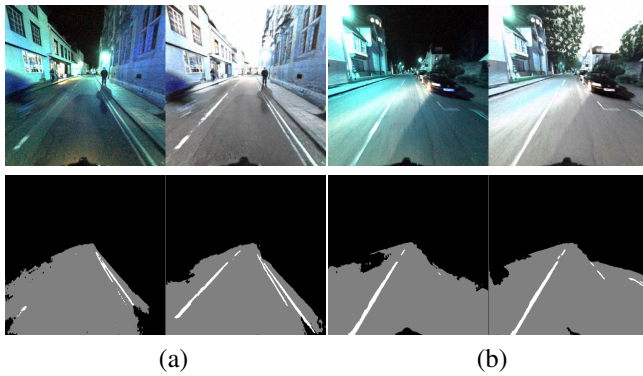


Fig. 12. Driveable area detection results before and after image enhancement. Images in the first row are the night image and the corresponding results enhanced by UMLE; the second row are the detection results of the drivable area of the corresponding images in the first row.

good conversion of image information and a more realistic detection of drivable areas as well as lane lines. By analyzing the performance, we can safely conclude that the proposed model can convert night scenes into day scenes in the same scene and improve the driveable area detection results very well.

IV. CONCLUSION

In this paper, we propose an unsupervised enhancement model for real-time low-light image enhancement. The model's training is independent of paired training data, so it can use images of different scenes and different illuminations. Besides, we present a multi-branch discriminator which can comprehensively evaluate the image from color, texture, and global information. We also introduce a novel attention module which combines the channel attention and the pixel attention to help to focus more on the low-light areas. Both qualitative and quantitative experimental evaluations show that our network achieves good results in terms of visual effects and noise control. In addition, we experimentally validate that our method is significantly more effective for tasks such as SLAM repositioning drivable area detection.

REFERENCES

- [1] S. M. Pizer, E. P. Amburn, J. D. Austin, R. Cromartie, and K. Zuiderveld, "Adaptive histogram equalization and its variations," *Computer Vision Graphics & Image Processing*, vol. 39, no. 3, pp. 355–368, 1987.
- [2] H. Ibrahim and N. S. P. Kong, "Brightness preserving dynamic histogram equalization for image contrast enhancement," *IEEE Transactions on Consumer Electronics*, vol. 53, no. 4, pp. 1752–1758, 2008.
- [3] C. Lee, C. Lee, and C. Kim, "Contrast enhancement based on layered difference representation of 2d histograms," *IEEE Trans. Image Process.*, vol. 22, no. 12, pp. 5372–5384, 2013.
- [4] E. H. Land, "The retinex theory of color vision," *Scientific american*, vol. 237, no. 6, pp. 108–129, 1977.
- [5] D. J. Jobson, Z. Rahman, and G. A. Woodell, "A multiscale retinex for bridging the gap between color images and the human observation of scenes," *IEEE Transactions on Image processing*, vol. 6, no. 7, pp. 965–976, 1997.

- [6] X. Guo, "LIME: A method for low-light image enhancement," in *Proceedings of the 2016 ACM Conference on Multimedia Conference*, A. Hanjalic, C. Snoek, M. Worring, D. C. A. Bulterman, B. Huet, A. Kellihier, Y. Kompatsiaris, and J. Li, Eds., 2016, pp. 87–91.
- [7] K. Nakai, Y. Hoshi, and A. Taguchi, "Color image contrast enhancement method based on differential intensity/saturation gray-levels histograms," in *International Symposium on Intelligent Signal Processing and Communication Systems*, 2013, pp. 445–449.
- [8] Z. Ying, G. Li, and W. Gao, "A bio-inspired multi-exposure fusion framework for low-light image enhancement," *CoRR*, vol. abs/1711.00591, 2017.
- [9] K. G. Lore, A. Akintayo, and S. Sarkar, "Llnet: A deep autoencoder approach to natural low-light image enhancement," *Pattern Recognition*, vol. 61, pp. 650–662, 2015.
- [10] C. Wei, W. Wang, W. Yang, and J. Liu, "Deep retinex decomposition for low-light enhancement," *arXiv preprint arXiv:1808.04560*, 2018.
- [11] C. Chen, Q. Chen, J. Xu, and V. Koltun, "Learning to see in the dark," in *Proceedings of the IEEE Conference on Computer Vision and Pattern Recognition*, 2018, pp. 3291–3300.
- [12] Y. Zhang, J. Zhang, and X. Guo, "Kindling the darkness: A practical low-light image enhancer," in *Proceedings of the 27th ACM International Conference on Multimedia*, 2019, pp. 1632–1640.
- [13] Y. Qu, Y. Ou, and R. Xiong, "Low illumination enhancement for object detection in self-driving," in *2019 IEEE International Conference on Robotics and Biomimetics (ROBIO)*. IEEE, 2019, pp. 1738–1743.
- [14] R. Chen, W. Huang, B. Huang, F. Sun, and B. Fang, "Reusing discriminators for encoding: Towards unsupervised image-to-image translation," in *2020 IEEE/CVF Conference on Computer Vision and Pattern Recognition*, 2020, pp. 8165–8174.
- [15] J. Hu, L. Shen, S. Albanie, G. Sun, and E. Wu, "Squeeze-and-excitation networks," *IEEE Trans. Pattern Anal. Mach. Intell.*, vol. 42, no. 8, pp. 2011–2023, 2020.
- [16] Q. Wang, B. Wu, P. Zhu, P. Li, W. Zuo, and Q. Hu, "Eca-net: Efficient channel attention for deep convolutional neural networks," in *2020 IEEE/CVF Conference on Computer Vision and Pattern Recognition, CVPR*. IEEE, 2020, pp. 11 531–11 539.
- [17] A. Anoosheh, T. Sattler, R. Timofte, M. Pollefeys, and L. Van Gool, "Night-to-day image translation for retrieval-based localization," in *2019 International Conference on Robotics and Automation (ICRA)*. IEEE, 2019, pp. 5958–5964.
- [18] Y. Jiang, X. Gong, D. Liu, Y. Cheng, C. Fang, X. Shen, J. Yang, P. Zhou, and Z. Wang, "Enlightengan: Deep light enhancement without paired supervision," *CoRR*, vol. abs/1906.06972, 2019.
- [19] X. Mao, Q. Li, H. Xie, R. Y. K. Lau, Z. Wang, and S. P. Smolley, "Least squares generative adversarial networks," in *IEEE International Conference on Computer Vision, ICCV*. IEEE Computer Society, 2017, pp. 2813–2821.
- [20] N. K. Kalantari and R. Ramamoorthi, "Deep high dynamic range imaging of dynamic scenes," *ACM Trans. Graph.*, vol. 36, no. 4, pp. 144:1–144:12, 2017.
- [21] X. Glorot, A. Bordes, and Y. Bengio, "Deep sparse rectifier neural networks," in *Proceedings of the Fourteenth International Conference on Artificial Intelligence and Statistics*, vol. 15, 2011, pp. 315–323.
- [22] H. Yong, J. Huang, X. Hua, and L. Zhang, "Gradient centralization: A new optimization technique for deep neural networks," *CoRR*, vol. abs/2004.01461, 2020.
- [23] J. Kim, M. Kim, H. Kang, and K. Lee, "U-gat-it: unsupervised generative attentional networks with adaptive layer-instance normalization for image-to-image translation," *arXiv preprint arXiv:1907.10830*, 2019.
- [24] X. Huang and S. J. Belongie, "Arbitrary style transfer in real-time with adaptive instance normalization," in *IEEE International Conference on Computer Vision, ICCV*. IEEE Computer Society, 2017, pp. 1510–1519.
- [25] L. J. Ba, J. R. Kiros, and G. E. Hinton, "Layer normalization," *CoRR*, vol. abs/1607.06450, 2016.
- [26] F. Lv, F. Lu, J. Wu, and C. Lim, "MBLLEN: low-light image/video enhancement using cnns," in *British Machine Vision Conference 2018*, 2018, p. 220.
- [27] J.-Y. Zhu, T. Park, P. Isola, and A. A. Efros, "Unpaired image-to-image translation using cycle-consistent adversarial networks," in *Proceedings of the IEEE international conference on computer vision*, 2017, pp. 2223–2232.
- [28] W. Wang, C. Wei, W. Yang, and J. Liu, "Gladnet: Low-light enhancement network with global awareness," in *13th IEEE International Conference on Automatic Face & Gesture*, 2018, pp. 751–755.

- [29] A. Mittal, Fellow, IEEE, R. Soundararajan, and A. C. Bovik, "Making a 'completely blind' image quality analyzer," *IEEE Signal Processing Letters*, vol. 20, no. 3, pp. 209–212, 2013.
- [30] J. R. A, "Focus optimization criteria for computer image processing [j]," in *Microscope*, 1976, pp. 163–180.
- [31] S. Park, T. Schöps, and M. Pollefeys, "Illumination change robustness in direct visual slam," in *ICRA*, 2017.
- [32] R. Mur Artal and J. D. Tardós, "ORB-SLAM2: an open-source SLAM system for monocular, stereo and RGB-D cameras," *IEEE Transactions on Robotics*, vol. 33, no. 5, pp. 1255–1262, 2017.
- [33] J. Redmon and A. Farhadi, "Yolov3: An incremental improvement," *CoRR*, vol. abs/1804.02767, 2018. [Online]. Available: <http://arxiv.org/abs/1804.02767>